Advanced electron tomography of nanoparticle assemblies

Advanced electron tomography of nanoparticle assemblies

T. ALTANTZIS, D. ZANAGA and S. BALS[(a)]

EMAT, University of Antwerp –Groenenborgerlaan 171, B-2020 Antwerp, Belgium

received and accepted dates provided by the publisher
other relevant dates provided by the publisher

PACS 87.64.Ee – Electron microscopy
PACS 81.16.Dn – Self-assembly
PACS 81.70.Tx – Computed tomography

Abstract – Nanoparticle assemblies have attracted enormous scientific interest during the last years, due to their unique properties compared to those of their building blocks. To understand the origin of these properties and to establish the connection with their structure, a detailed and quantitative structural characterization is essential. Transmission electron microscopy has been widely used to investigate nano-assemblies. However, TEM images only correspond to a two-dimensional projection of a three-dimensional object. Therefore, in order to obtain the necessary 3D structural information electron tomography has to be applied. By means of advanced electron tomography, both qualitative and quantitative information can be obtained, which can be used for detailed theoretical studies.

Introduction – Assemblies of nanoparticles have recently gained increasing interest due to their improved properties compared to those of their building blocks. By varying the size and the shape of the nanoparticles as well as the synthesis parameters, assemblies with unique configurations can be obtained, yielding applications in different scientific fields including plasmonics, [1] signal enhancement, [2,3] sensoric, [4] catalysis [5,6] and data storage [7,8]. Although the behaviour of such assemblies is empirically understood, thorough insight on the structure-property connection is often still lacking. A detailed structural characterization is therefore of utmost importance.

Transmission electron microscopy (TEM) is a well-known technique to characterize materials at the nanometre scale and below. However, it conventionally only allows for the acquisition of 2D projections of 3D objects, which is not sufficient for a quantitative characterization of complex 3D nanostructures. To overcome this limitation, electron tomography, a technique during which 2D projections are acquired over a large tilt range and combined through the use of a mathematical reconstruction algorithm, has been developed [9]. Over the last decennia, electron tomography has developed into a powerful characterization tool that has been widely used in the field of materials science. Mostly, electron tomography is based on high angle annular dark field scanning transmission electron microscopy (HAADF-STEM) [10]. Using HAADF-STEM, the image intensity scales with the thickness of the samples and with the atomic number Z of the elements that are present [11]. In this manner, the morphology of a broad range of nanomaterials has been investigated. Tomography has furthermore been combined with spectroscopic techniques such as electron energy loss spectroscopy (EELS) [12-14] and energy dispersive X-ray spectroscopy (EDS) [15-18], which enabled the 3D investigation of chemical composition, bonding nature and surface plasmons of nanomaterials. In addition, great effort was made to develop advanced reconstruction algorithms, enabling quantification of the 3D results and pushing the resolution of the technique to the atomic scale [19-22].

Electron tomography is nowadays also a standard technique for the characterization of nano-assemblies, yielding a description of the morphology and inner structure (fig. 1) [23-27]. In this perspective, we will provide an overview of the latest progress and the future challenges in the field of 3D characterization of nano-assemblies using electron tomography. Indeed, one of the current goals is to investigate more complex or larger assemblies of nanoparticles in a quantitative manner. A quantitative description of the assemblies is required to determine the number of particles in the assembly and the position of the individual nanoparticles in 3D. Based on this information, the stacking of the system, inter-particle distances and outer morphology can be studied. Such an investigation allows a comparison with theoretical models and a better understanding of the mechanisms which rule the self-assembling process. Finally, we will provide an outlook and will describe future opportunities.

History and basic principles of electron tomography – Electron tomography has been applied in the biological sciences since the 70s, but the resolution was limited to the nanometre range because of several parameters such as beam damage, the thickness of the sample and the demanding sample preparation. When investigating inorganic materials, beam damage might be a bottleneck for specific samples, but there are even more important problems to overcome. Indeed, conventional bright field TEM (BF-TEM) images of

[(a)]E-mail: sara.bals@uantwerpen.be

crystalline materials are often dominated by Bragg scattering and for certain orientations, the interaction is non-linear. This violates the so-called *projection requirement*, which states that the intensity of each image of a tomographic tilt series should be a monotonic function of a physical property of the sample under investigation [28]. Therefore, it is only during the last 15 years that electron tomography has been introduced in materials sciences. One of the earliest studies demonstrating bright field tomography for the reconstruction of porous zeolites was published by Koster and co-workers [29]. However, the presence of diffraction contrast in BF-TEM images of crystalline materials hampered the application of the technique to metallic nanostructures. The development of electron tomography based on HAADF-STEM images led to the possibility of characterizing crystalline nanoparticles in 3D as well [10,30]. Ever since, the technique has been used in numerous studies. A great advantage of the technique is that, the intensity in the projections is proportional to Z^n ($1.6 < n < 2$) [11]. Therefore, not only structural, but also chemical information can be obtained.

During a conventional electron tomography experiment, a tilt series of projection images is acquired by tilting the sample in between the pole pieces of the objective lens over a large tilt range, with a tilt increment of typically 1º or 2º (see figs. 1a and 1b). Next, the tilt series of projection images is aligned using fiducial markers or cross-correlation. Finally, by using a mathematical algorithm, the tilt series is combined into a 3D reconstruction of the original object (see fig. 1c). However, due to the limited space between the two pole pieces of the objective lens or because of shadowing effects that appear at high tilt angles, it is not possible to tilt the sample over the full tilt range of 180º. As a result, a so-called *missing wedge* of information will be present, leading to artefacts in the final reconstruction of which an elongation in the direction along the *missing wedge* is the most prominent. Obviously, this severely hampers a quantitative interpretation of the results.

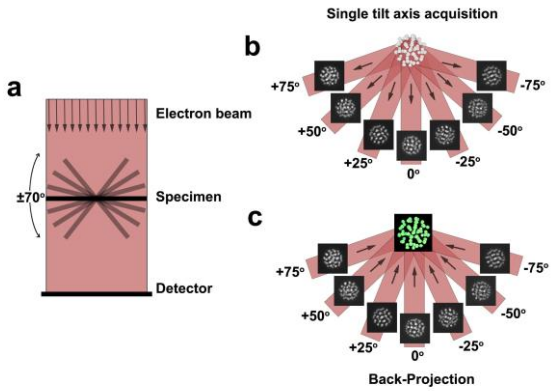

Fig. 1: (Colour on-line) A schematic illustration of a continuous electron tomography experiment, including the acquisition of a tilt series (a and b) and back projection of the images along their original acquisition directions (c).

In order to reduce *missing wedge* artefacts, different acquisition geometries can be used. The *dual-tilt axis* tilt scheme is based on the acquisition of two tilt series, acquired along two tilt axes that are perpendicular to each other. By merging both reconstructions, the *missing wedge* is reduced to a *missing pyramid* [31-33]. However, a major limitation is the fact that this requires twice the electron dose, which might lead to beam damage. Another alternative is the so-called *on-axis tilt* geometry. Hereby, a needle shaped sample is attached at the end of a dedicated on-axis tomography holder enabling a 360º tilt [34-36]. Such needle-shaped samples can be prepared by focussed ion beam (FIB) milling. Although there have been recent studies in which the technique was also applied to image nanoparticles in 3D, the technique is generally not applicable to nano-assemblies [37].

As described above, after the acquisition of a tilt series, a mathematical algorithm is used to obtain a 3D reconstruction of the original object. When using the *direct back projection* method, the projection images of a tilt series are all re-projected along the original acquisition angles and the superposition will yield the final reconstruction [9,38]. However, reconstructions that are obtained in this manner are blurred due to an enhancement of the low frequencies. This can be avoided by the use of different weighting filters and the technique is called *weighted back projection*. With the increase of computing power, iterative reconstruction approaches became more commonly used. A well-known algorithm is the simultaneous iterative reconstruction technique (SIRT), where the reconstruction quality is improved by minimizing the difference between the forward projections of an intermediate reconstruction and the original projections in an iterative manner [39]. These conventional reconstruction algorithms do not use any prior information on the sample that needs to be reconstructed. In this manner, the quality of the final result is predominantly determined by the number of projection images and the angular range over which they are acquired. As illustrated by the examples below, it is safe to state that despite these difficulties, electron tomography has evolved into a standard tool for the characterization of nano-assemblies, yielding a description of the morphology and inner structure.

Qualitative electron tomography for assemblies – As a first example, we present a detailed structural and morphological characterization of assemblies of polysterene (PS)-stabilized spherical Au nanoparticles. The Au nanoparticles, which are dispersed in tetrahydrofuran (THF) can form aggregates upon the addition of water. The procedure is further explained in ref. [23]. The influence of the modification of different parameters, such as the size of the Au nanoparticles as well as the length of the polymer chains, on the modulation of the hydrophobic interactions was studied. Therefore, nine different samples were investigated, where these two parameters were modified. Tilt series were acquired in HAADF-STEM mode and the reconstruction was performed by using the SIRT algorithm.

In fig. 2, 3D representations of the reconstructed volumes are given for each sample. Based on the electron tomography results, the spatial distribution, the number of the particles in the assemblies, as well as inter-particle distances can be extracted. From the analysis of these parameters a certain degree of order could be revealed. Furthermore, by varying the length of the polymer chains it was possible to modulate the gap distances between the particles. Regardless of particle diameter, for the shortest polymer chain length, the distances were smaller (2-5 nm) as compared to the longest polymer chains, where the distances were 19-22 nm respectively. These findings render the clusters accessible for molecular uptake and controlled release, which may have interesting biological applications. Furthermore, regardless of the mean nanoparticle diameter, an increase of the length of the PS chains induces an increase of the redshift of the plasmon band. This feature brings new insights into the field of plasmon engineering, suggesting that the plasmonic optical window can be easily tuned independently of the available space between the particles.

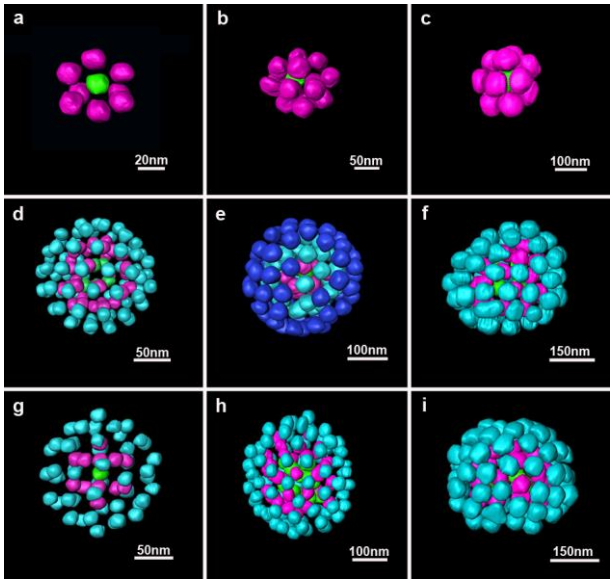

Fig. 2: (Colour on-line) 3D representation of the reconstructed assemblies, where the different shells of Au nanoparticles in each assembly are represented with different colours [23].

Also for 2D superlattices, electron tomography is of great interest. Indeed, controlled oriented attachment is currently emerging as a route to form extended one- and two-dimensional single crystalline semiconductors of II-VI and IV-VI compounds [40-44]. Truncated nanocubes of the Pb-chalcogenide family have been recently used to create 2D atomically coherent superlattices with square or honeycomb geometries [44]. In fig. 3a, it can be seen that honeycomb structures with long-range periodicity can be obtained [26]. The high resolution image, presented in fig. 3b, reveals that the ⟨111⟩ axes of the NCs are perpendicular to the substrate and that the NC-NC bonds are perpendicular to three of the ⟨110⟩ axes. Three were the possible models for attachment of the NCs that could result in a honeycomb structure with the nanocrystal ⟨111⟩ axes perpendicular to the substrate: attachments via the {110}, {111}, or {100} facets, respectively (figs. 3d-i). The three structures appear similar from the top but have a very different 3D geometry. Therefore, electron tomography is required. The acquisition of the tilt series was performed in HAADF-STEM mode and the reconstruction was performed using the SIRT algorithm. Slices through the reconstruction in the direction perpendicular to the substrate indicate that the two inequivalent NCs in the honeycomb unit cell are located on different heights as indicated in figs. 3k and 3l. A 3D visualisation and a schematic illustration are presented in figs. 3m and 3n respectively. It should be noted that the HAADF-STEM projections in fig. 3j show a hexagonal structure, resembling a *graphene* type of arrangement. It is only by applying electron tomography that a *silicine* type of arrangement could be revealed. These results therefore prove that also for 2D like assemblies, 2D TEM images are not sufficient to interpret the complete structure.

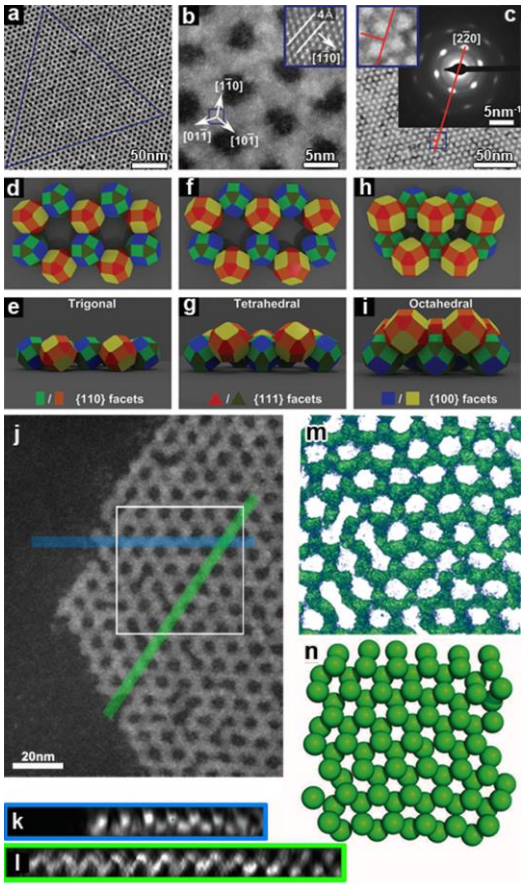

Fig. 3: (Colour on-line) a) HAADF-STEM image of the honeycomb structure. The equilateral triangle shows the long-range ordering of the structure. b) High-resolution HAADF-

STEM image showing that the ⟨111⟩ NC axes are perpendicular to the honeycomb plane, and three of the ⟨110⟩ axes are perpendicular to the NC bonds. (Inset) Zoom-in on the atomic columns indicated by the blue box. c) Electron diffraction pattern showing the high degree of crystallinity. TEM image in the background shows the area on which the ED pattern was recorded. Red line and inset show the orientation of the diffraction spots with respect to the honeycomb structure, confirming that the ⟨110⟩ axes are perpendicular to the NC bonds. d-i) Models of the honeycomb structure, with cantellated cubes as nanocrystals. The two inequivalent sites in the honeycomb lattice are indicated by yellow/red and blue/ green NCs. Rectangles (orange and light green) represent {110} facets, triangles (red and dark green) represent {111} facets, and squares (yellow, blue) represent {100} facets. d) and e) are the top and side view of the trigonal structure, respectively. f) and g) are top and side view of the tetrahedral structure, respectively. h) and i) are the top and side view of the octahedral structure, respectively. j) HAADF-STEM projection of a planar assembly of PdSe nanoparticles. k) and l) Slices through the SIRT tomographic reconstruction of the assembly in (j), along the directions highlighted by the blue and green bars. m) Reconstruction rendering of the structure and n) equally sized spheres plotted on the coordinates obtained by automated particle detection in the region indicated in white in panel (j) [26].

Electron tomography was recently also applied to gold nanorod super-crystals with varying numbers of stacked layers [1]. In fig. 4, an example of such a structure with two layers on top of each other is presented. Such systems find a broad interest in fields ranging from sensor design to catalysis and light harvesting systems and are furthermore of interest in plasmon enhanced spectroscopy [45]. By using electron tomography, we could confirm the ABA-type stacking (see fig. 4) and moreover, it was possible to reveal the presence of a misorientation of the gold nanorod layers. The results are of great importance since they could be used to connect the structure to the optical properties.

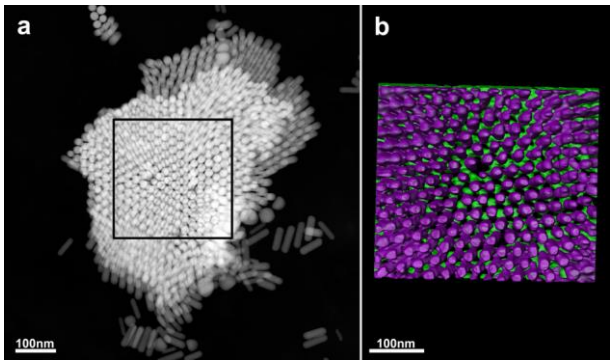

Fig. 4: (Colour on-line) a) HAADF-STEM image of a bilayer super-crystal of standing gold nanorods b) 3D representation of the reconstructed volume of the part of the bilayer indicated by the black square in (a), showing the top and bottom layers in purple and green colours respectively [1].

Quantitative electron tomography for assemblies – Several groups have demonstrated the ability to investigate nanoparticle assemblies by electron tomography [24-26]. Hereby, either BF-TEM or HAADF-STEM was used to obtain the series of 2D images. However, the demand in the field of electron tomography is nowadays evolving from qualitative visualisations to quantitative measurements of properties such as morphologies or chemical compositions. Indeed, reliable quantification of the structural parameters enables a direct comparison of data and models for the self-assembly of particles, obtained through simulations [46].

To extract quantitative information, optimization of the electron tomography experiment is required. This is especially the case for large assemblies that have a thickness > 500 nm. For such systems, the conventional approaches yield different types of artefacts hampering a quantitative interpretation of the 3D data. One of the bottlenecks concerns the so-called *cupping artefact*, which is related to an increase of multiple scattering and backscattering for relatively thick samples. Consequently, a smaller amount of the incoming electron beam is scattered towards the detector, leading to an underestimation of the intensity. As a consequence, both a qualitative and quantitative interpretation of the results are no longer straightforward. We recently proposed the use of incoherent BF-STEM to overcome this problem [47,48].

An additional problem is that in order to extract quantitative data from a 3D reconstruction, a segmentation step is required to determine the correspondence between different grayscales in the reconstruction and different compositions in the original structure. Automatic segmentation by using a threshold at different grey levels is hampered by *missing wedge* artefacts and quantitative interpretation based on the conventional 3D reconstruction algorithms is therefore quite difficult. For relatively small assemblies of closed-packed nanoparticles (consisting of 100 particles or less), the number of particles can be determined and their coordinates can be estimated manually [23]. However, if the number of particles increases and the distance between them is less than the 3D resolution of the tomography experiment [49], a manual segmentation becomes subjective and reliable quantification of the data is impossible. As an example, fig. 5a shows a SIRT reconstruction for an assembly of iron cobalt oxide nanoparticles, obtained by spherical confinement [50], with a single nanoparticle diameter of 6 nm and a total diameter of approximately 300 nm. A slice through the reconstruction (fig. 5b) shows the effect of *missing wedge* artefacts (red rectangle) hampering the distinction of the single nanoparticles. In order to extract the coordinates of the particles, the only possibility would be to attempt a manual segmentation, which would prove highly challenging, tedious and subjective.

It must be noted that none of the conventional reconstruction algorithms such as *weighted back projection* and SIRT uses additional information on the system that one wants to reconstruct. By implementing *a priori* knowledge, the quality of a reconstruction can be drastically improved and very often, such additional information on the sample is indeed

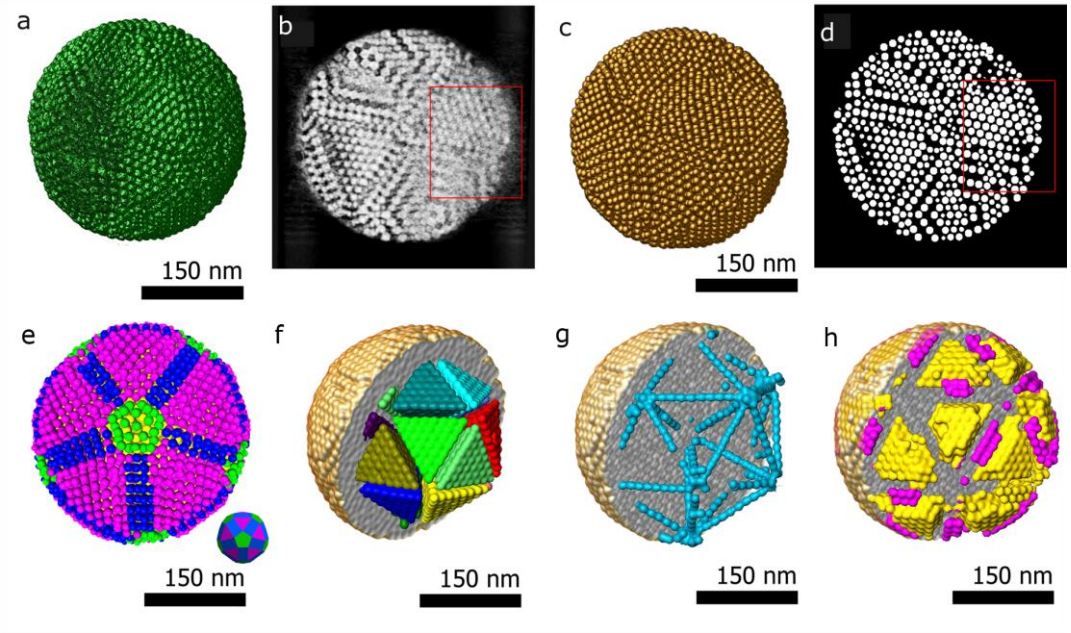

Fig. 5: (Colour on-line) Assembly of iron cobalt oxide nanoparticles. a) SIRT reconstruction rendering, b) slice through the SIRT reconstruction. c) Shape model basis reconstruction rendering, d) slice through the optimized reconstruction. e) Surface particles segmented based on the different facets highlighting the rhombicosidodecahedral structure. f) Inner Mackay icosahedron, composed by 20 tetrahedra of particle in an fcc stacking. g) Particles showing icosahedral symmetry. h) Anti-Mackay surface termination, particles in fcc stacking [56].

available or can be obtained using other TEM techniques. Different approaches already exist, such as discrete tomography [51,52] and techniques based on compressed sensing [53-55]. However, these advanced approaches do not work well for nano-assemblies since blurring always occurs and the *missing wedge* leads to a superposition of the particle boundaries, hampering to distinguish them. This is particularly the case for large assemblies of spherical particles or when only a limited number of projections are available. It must be noted that during the 3D investigation of an assembly of nanoparticles, the exact shape of the individual particles is often not of crucial interest and we can assume that they correspond to perfect spheres. If the size of the particles can be estimated, we can use discrete spheres as basis elements and the problem is reduced to the reconstruction of the centre coordinates of these spheres. In this manner, the tomographic problem can be reformulated using a new shape model basis. Solving this new tomographic problem yields directly the coordinates of each particle, from which the full structure can be recovered by convolving the coordinates with the function used as basis. A 3D visualisation of a reconstruction obtained using this approach, as well as an orthoslice is shown in figs. 5c and d. Comparison with figs. 5a and b immediately highlights the improvement over the SIRT reconstruction, especially in recovering the lost information due to the *missing wedge* artefacts [56].

Once the particle coordinates are obtained, further investigations on the assembly structure can be performed by analysing the bond order parameters [57,58], which enable the detailed identification of the assembly structure, including the packing of the particles and its symmetry. Figure 5e highlights the surface facets forming a rhombicosidodecahedron, whereas fig. 5f shows the icosahedral core identified as the assembly core, composed by 20 tetrahedra, each of which is made up of particles in a face centered cubic (fcc) packing. Each tetrahedron is separated by a twinning plane of hexagonal closed packed (hcp) particles. Along the edges of the tetrahedra, particles with icosahedral symmetry are detected (fig. 5g) and finally, fig. 5h shows the fcc particles composing the surface termination. The detailed analysis of this assembly of 9301 nanoparticles is an example of quantitative characterization that is made possible by electron tomography and a combination of optimized acquisition and reconstruction of the tilt series [56].

The same technique was used to characterize assemblies of iron oxide nanoparticles obtained through an innovative synthesis route, and resulting in peculiar structures consisting of a spherical layer of nanoparticles, half-filled by closely packed nanoparticles and embedded in silica [59]. The approach also holds great potential for the reconstruction of less complex assemblies (less particles in a non-closed packed arrangement) from a very limited amount of projections. In this manner, the acquisition time and the required electron dose can be greatly reduced, which therefore opens the route to the quantitative analysis of beam sensitive assemblies. Since nanoparticle assemblies by definition mostly consist of repetitive building blocks (spheres, nanorods, nanocubes and others) the idea to include prior knowledge about the shape can be extended to these other types of nanoparticle assemblies as well. The approach therefore presents itself as a powerful and promising method for the future developments in the field of quantitative characterization of complex nanoparticles assemblies.

Future challenges – Binary assemblies, which can be formed by particles with different sizes and shapes or particles with different composition, are of high importance because they provide even more flexibility to produce to metamaterials with potentially new collective chemical or physical properties. At the same time, the 3D characterization of such systems will be increasingly more complex. This is definitely true if one wants to investigate assemblies consisting of elements with a small difference in atomic number Z (such as Fe-Co or Au-Pt). For such samples, 3D HAADF-STEM reconstructions will no longer enable one to distinguish between the different types of particles. An alternative approach is therefore the use of EDS tomography. So far, EDS tomography was hampered by experimental limitations such as the sample-EDS detector geometry and the shadowing of half the tilt series [15].

Novel detector set-ups have, however, enabled the extension of EDS from 2D to 3D. We recently developed a quantitative 3D reconstruction approach for EDS, based on the *ζ-factor method* [60,61]. This method was originally developed for the chemical quantification of thin films, but the combination with HAADF-STEM electron tomography will enable us to extend its use to nanoparticle assemblies.

Going even further is the investigation of the assemblies at the atomic scale. Most high-resolution studies in 3D have been carried out for relatively stable materials. Unfortunately, for many assemblies, it is far from straightforward to acquire a large number of TEM images since samples tend to degrade or deform under the electron beam. This is certainly the case for the honeycomb assemblies as illustrated in fig. 6. Estimation of 3D models from single 2D projection images is therefore gaining renewed interest.

Using the atom counting procedure that was introduced in ref. [62], it was recently shown that the number of atoms in a given atomic column can be counted with single atom sensitivity from annular dark field (ADF) STEM images. The technique is based on a statistical analysis of so-called scattering cross sections, which can be obtained at the atomic level when using an empirical model-based approach. Next, the counting results can be used to generate a starting configuration where each atomic column is positioned symmetrically around a central plane. Using a Monte-Carlo based energy minimization, a 3D model for the structure of the nanoparticle can be proposed [19]. We recently used this approach to study the interface between individual PbSe building blocks in a 2D superlattice formed by oriented attachment (see fig. 6) [63].

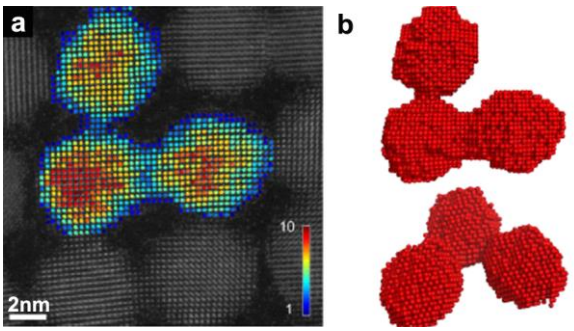

Fig. 6: (Colour on-line) a) HAADF-STEM image of PbSe nanocrystals attached in a square superlattice, overlaid with results from the atom counting procedure, revealing the type of connection between the crystals. The colour bar represents the number of atoms in each column. b) The reconstructed atomic model along different viewing directions [63].

Summary – Electron tomography has been used in an increasing number of studies to investigate the 3D structure of assemblies of nanomaterials. Recent advances have enabled us to extract quantitative information, which is of great importance to optimize the synthesis and establish the connection between the structure and the properties of the nano-assemblies. One of the future challenges will be to also investigate binary assemblies and to push the resolution of these approaches to the atomic level. The ability to investigate assemblies by electron tomography can be considered as the start of a new journey in the field of 3D electron microscopy and materials science in general.

***

We would like to thank the colleagues who have contributed to this work over the years, including L. M. Liz-Marzán, M. Grzelczak, A. Sánchez-Iglesias, D. Vanmaekelbergh, M. P. Boneschanscher, W. H. Evers, J. J. Geuchies, B. Goris, A. de Backer, S. van Aert, M.-P. Pileni, Z. Yang, K. J. Batenburg, J. Sijbers, F. Bleichrodt, W. J. Palenstijn, A. van Blaaderen, M. A. van Huis, F. M. Peeters, N. Winckelmans and D. Wang. The authors gratefully acknowledge funding from the Research Foundation Flanders (G.0381.16N, G.036915 G.0374.13 and funding of a postdoctoral grant to T.A). S.B. and D.Z. acknowledge funding from the European Research Council, ERC grant N°335078 – Colouratom.

REFERENCES

[1] HAMON C. *et al., ACS Photonics*, **2** (2015) 1482.
[2] GUO S. *et al., J. Mater. Chem.*, **21** (2011) 16704.
[3] KIM K. *et al., Phys. Chem. Chem. Phys.*, **12** (2010) 3747.
[4] XU L. *et al., J. Mater. Chem.*, **21** (2011) 16759.
[5] XU Y. *et al., Chem. Commun.*, **48** (2012) 2665.

[6] GUO S. *et al., J. Am. Chem. Soc.*, **134** (2012) 2492.
[7] PILENI M.P. *et al., J. Mater. Chem.*, **21** (2011) 16748.
[8] PILENI M.-P. *et al., Nat. Mater.*, **2** (2003) 145.
[9] HOPPE W. *et al., Naturwissenschaften.*, **55** (1968) 333.
[10] MIDGLEY P.A. *et al., Ultramicroscopy.*, **96** (2003) 413.
[11] PENNYCOOK S.J. *et al., Ultramicroscopy.*, **30** (1989) 58.
[12] YEDRA L. *et al., Ultramicroscopy*, **122** (2012) 12.
[13] GORIS B. *et al., ACS Nano*, **8** (2014) 10878.
[14] NICOLETTI O. *et al., Nature*, **502** (2013) 80.
[15] MÖBUS G. *et al., Ultramicroscopy*, **96** (2003) 433.
[16] BALS S. *et al., Angew. Chemie - Int. Ed.*, **53** (2014) 10600.
[17] LIAKAKOS N. *et al., Nano Lett.*, **14** (2014) 2747.
[18] LEPINAY K. *et al., Micron*, **47** (2013) 43.
[19] VAN AERT S. *et al., Nature*, **470** (2011) 374.
[20] CHEN C.-C. *et al., Nature*, **496** (2013) 74.
[21] GORIS B. *et al., Nat. Mater.*, **11** (2012) 930.
[22] BALS S. *et al., Nano Lett.*, **11** (2011) 3420.
[23] SÁNCHEZ-IGLESIAS A. *et al., ACS Nano*, **6** (2012) 11059.
[24] FLOREA I. *et al., ACS Nano*, **6** (2012) 2574.
[25] FRIEDRICH H. *et al., Nano Lett.*, **9** (2009) 2719.
[26] BONESCHANSCHER M.P. *et al., Science*, **344** (2014) 1377.
[27] GRZELCZAK M. *et al., Nano Lett.*, **12** (2012) 4380.
[28] HAWKES P. W. *et al., in Electron Tomography: Three dimensional imaging with the transmission electron microscope*, in: J. Frank (Ed.), (Pleum, New York, London) 1992.
[29] KOSTER A.J. *et al., J. Phys. Chem. B.*, **104** (2000) 9368.
[30] MIDGLEY P.A. *et al., Chem. Commun.*, (2001) 907.
[31] ARSLAN I. *et al., Ultramicroscopy*, **106** (2006) 994.
[32] RADERMACHER M. *et al., J. Electron Microsc. Tech.*, **9** (1988) 359.
[33] VAN AARLE W. *et al., Ultramicroscopy*, **157** (2015) 35.
[34] BIERMANS E. *et al., Nano Lett.*, **10** (2010) 5014.
[35] KE X. *et al., Microsc. Microanal.*, **16** (2010) 210.
[36] KAWASE N. *et al., Ultramicroscopy*, **107** (2007) 8.
[37] JARAUSCH K. *et al., J. Electron Microsc. (Tokyo)*, **58** (2009) 175.
[38] CROWTHER R.A. *et al., Proc. R. Soc. A Math. Phys. Eng. Sci.*, **317** (1970) 319.
[39] GILBERT P. *et al., J. Theor. Biol.*, **36** (1972) 105.
[40] PACHOLSKI C. *et al., Angew. Chemie - Int. Ed.*, **41** (2002) 1188.
[41] CHO K.S. *et al., J. Am. Chem. Soc.*, **127** (2005) 7140.
[42] KOH W.K. *et al., J. Am. Chem. Soc.*, **132** (2010) 3909.
[43] SCHLIEHE C. *et al., Science*, **329** (2010) 550.
[44] EVERS W.H. *et al., Nano Lett.*, **13** (2013) 2317.
[45] AROCA R.F. *et al., Phys. Chem. Chem. Phys.*, **15** (2013) 5355.
[46] GALVÁN-MOYA J.E. *et al., ACS Nano*, **8** (2014) 3869.
[47] ALTANTZIS T. *et al., Part. Part. Syst. Charact.*, **30** (2013) 84.
[48] ERCIUS P. *et al., Appl. Phys. Lett.*, **88** (2006).
[49] HEIDARI H. *et al., Ultramicroscopy*, **135** (2013) 1.
[50] DE NIJS B. *et al., Nat. Mater.*, **14** (2014) 56.
[51] BATENBURG K.J. *et al., Ultramicroscopy*, **109** (2009) 730.
[52] BALS S. *et al., J. Am. Chem. Soc.*, **131** (2009) 4769.
[53] GORIS B. *et al., Ultramicroscopy*, **113** (2012) 120.
[54] SAGHI Z. *et al., Nano Lett.*, **11** (2011) 4666.
[55] LEARY R. *et al., Ultramicroscopy*, **131** (2013) 70.
[56] ZANAGA D. *et al., Nanoscale*, **8** (2016) 292.
[57] STEINHARDT P.J. *et al., Phys. Rev. B.*, **28** (1983) 784.
[58] WANG Y. *et al., J. Chem. Phys.*, **122** (2005).
[59] YANG Z. *et al., J. Am. Chem. Soc.*, **138** (2016) 3493.
[60] ZANAGA D. *et al., Ultramicroscopy*, **164** (2016) 11.
[61] ZANAGA D. *et al., Part. Part. Syst. Charact.*, **33** (2016) 396.
[62] VAN AERT S. *et al., Ultramicroscopy*, **109** (2009) 1236.
[63] GEUCHIES J.J. *et al., Nat Mater.*, **15** (2016) 1248.